Advances in Molecular Relaxation and Interaction Processes, 24 (1982) 75—105
Elsevier Scientific Publishing Company, Amsterdam — Printed in The Netherlands

COMPUTER SIMULATION OF THE MOLECULAR DYNAMICS OF LIQUID DICHLORO METHANE [1]

M. W. EVANS and M. FERRARIO
Edward Davies Chemical Laboratories, University College of Wales, Aberystwyth SY23 1NE

(Received 29 March 1982)

ABSTRACT

The molecular dynamics of CH_2Cl_2 in the liquid state have been simulated with two model representations of the intermolecular potential. These consist of a 3 x 3 and 5 x 5 atom-atom simulation with or without fractional charges at the atomic sites. A variety of thermodynamical and spectroscopic results show that the 5 x 5 potential is the more accurate. The effect of adding charges is significant but not pronounced. For example the simulated far infra-red spectrum looks 15% more like the real thing after an attempt has been made to include charge-charge electrodynamics. It is clear, however, that a better representation of the intermolecular pair potential of CH_2Cl_2 is needed to match the far infra-red results, and this can probably be obtained by measurements of the second dielectric virial of CH_2Cl_2 over a sufficient temperature range. A coordinated experimental effort is needed to test the wide-range of simulated spectra now available for the asymmetric top CH_2Cl_2.

INTRODUCTION

Molecular dynamics and interactions in the liquid phase can now be investigated with an ever-increasing range of techniques. It is essential that a coordinated study of a suitable species be carried through before we can hope to assimilate the different viewpoints available. A particularly favourable liquid in this respect is dichloro methane, whose molecular dynamical properties have recently been reviewed in detail [1-3] This is particularly suitable for many areas of spectroscopy including inelastic neutron scattering, far infra-red, microwave infra-red

[1] This paper was presented at the Conference on Analytical and Computational Studies of Basic Problems in Molecular Liquids, held at the School of Theoretical Physics, Dublin Institute for Advanced Studies, 19-21 April 1982, under the auspices of the EUROPEAN MOLECULAR LIQUIDS GROUP.

0378-4487/82/0000—0000/$02.75

N.M.R., light scattering, non-linear electrooptics and Raman scattering. In principle these are all capable of providing time correlation functions [2] of various vectors or tensors associated with the movement of the molecule. Provided we know approximately the pair interaction potential between CH_2Cl_2 molecules then the technique of molecular dynamics simulation can be used to compute these correlation functions from the equation of motion. The problem of describing a range of spectra at a given state point is thus reduced to optimising the form of the pair interaction potential, and refining the techniques of computer simulation. If this process were then to be repeated at state-points over the complete range of existence of the liquid we would be in a better position to produce a predictive theory of the liquid state of molecular matter.

Unfortunately at present our knowledge of the potential energy surface between two interacting molecules the size of CH_2Cl_2 is very poor, despite the amount of painstaking work on the subject. This is due to a number of factors, not least among which is the difficulty of relating the pair potential to spectra from the liquid in a self-consistent manner, i.e. the need for a better potential has been obscured by the mathematical difficulties posed by liquid state molecular dynamics. Phenomenological theories (e.g. the generalised Langevin equation and variations) approach the pair-potential problem, if at all, at a glancing angle (e.g. some hydrodynamic approaches do not go into any detail about molecular interaction). However, one of the most sensitive methods of testing an intermolecular pair potential equation is through the second dielectric virial coefficient B_ε, and future measurements of B_ε for CH_2Cl_2 will be very useful.

In the absence of a quantitative expression for the potential energy of two interacting CH_2Cl_2 molecules computer simulation of this liquid relies on empirical forms. The most popular method at present is to represent the interaction between each atom of two distinct molecules by a Lennard-Jones form. The complete pair potential is a sum of atom-atom terms. This is supposed to cover the repulsive and dispersive components of the pair-potential. The electrodynamic components may be conveniently represented by fractional charges situated at each atomic site. This is much simpler than expanding the electrodynamic force field in multipole moments, especially for asymmetric tops such as CH_2Cl_2. The drawback of using charges has its roots in the technical difficulty at present of dealing with long-ranged interaction in a molecular dynamics simulation using periodic boundary conditions.

In this paper we describe a computer simulation of liquid CH_2Cl_2 using atom-atom forms for the pair-potential. We assume that the forces in the liquid are molecularly pairwise additive and produce a variety of time-correlation functions and atom-atom distribution functions suitable for comparison, at the same state

points, with freshly measured spectra of various kinds, should these become available. The paper is organised as follows. In section 1 we describe the two algorithms used: with respectively a 3 x 3 atom-atom potential (taking CH_2 as a moiety) and a fuller 5 x 5 atom-atom potential. In section 2 we present results with and without charge interactions. In section 3 we discuss these results in terms of the available experimental data and suggest ways in which a future coordinated project of experimental testing might develop.

SECTION 1: DESCRIPTION OF MOLECULAR DYNAMICS ALGORITHMS

TR12

This was developed from an algorithm written initially by Singer and Renaud. The equations of motion for 108 molecules are solved using a twostep predictor method based on a simple quadrature routine. The usual periodic boundary conditions are incorporated. In TR12 the CH_2Cl_2 molecule was represented by a 3 x 3 atom-atom potential with or without charges. The core atom-atom interaction is Lennard-Jones in type with parameters: $\sigma(Cl\text{-}Cl) = 3.35\mathring{A}$; $\sigma(CH_2\text{-}CH_2) = 3.96\mathring{A}$; $\varepsilon/k(Cl\text{-}Cl) = 173.5K$; $\varepsilon/k(CH_2\text{-}CH_2) = 70.5K$, taken from the literature [6].

The $Cl\text{-}CH_2$ interaction is evaluated using

$$\sigma(Cl\text{-}CH_2) = \tfrac{1}{2}(\sigma(Cl\text{-}Cl) + \sigma(CH_2\text{-}CH_2))$$

$$\frac{\varepsilon}{k}(Cl\text{-}CH_2) = \left(\frac{\varepsilon}{k}(Cl\text{-}Cl)\frac{\varepsilon}{k}(CH_2\text{-}CH_2)\right)^{\frac{1}{2}}$$

Partial charges were added so as to reproduce a total dipole moment of 1.6D. Thus the charge in the Cl unit is - 0.151e and that on the CH_2 unit is + 0.302e. The full potential (atom-atom + charges) has been tested out by McDonald [4] at 287K (a molar volume of 62.92 cm^3/mole), and gave a mean potential energy of -6.2 kcal/mole, which compares well with the measured value [5] of -6.2 kcal $mole^{-1}$ to -6.3 kcal $mole^{-1}$ estimated from experimental ΔH values of 6.69 to 6.83 kcal $mole^{-1}$ in the literature [5]. About 0.5 kcal $mole^{-1}$ has been allowed for the $\Delta(PV)$ term. From this indication it seems that the main features of the force field are correct within what turns out to be (below) the quite severe limitations of the three-unit potential model for CH_2Cl_2 pair interactions in the liquid state. Insofar as the Lennard-Jones parameters used are taken from those in the literature it seems that these are to a degree transferable and in this sense there are no free parameters in the 3 x 3 model. The runs were carried out mainly at 293K, 1 bar, V = 64.0 cm^3 $mole^{-1}$. (This is a European Molecular Liquids Group pilot project state point [2,3] for CH_2Cl_2).

The molecular dynamics runs were carried out with a time step of 5 x 10^{-15} sec (0.005 ps). The initial equilibration runs usually required about 2500 time steps for satisfactory energy conservation (rotational and translational). These were

rejected and information from the next 2000 time steps stored on magnetic tape at intervals of 3 time steps. Temperatures were rescaled to stop drifts of more than 25K either side of the intial 293K. This information was used to construct time auto-correlation functions of various kinds with the usual running-time averaging. A.c.f.'s were constructed of: $\underline{v}$, the centre of mass linear velocity; J the angular momentum; $\underline{e}_A$ the dipole unit vector; $\underline{e}_B$ and $\underline{e}_C$, unit vectors along the orthogonal, principal moment of inertia axes, and from the derivatives $\dot{\underline{e}}_A$, $\dot{\underline{e}}_B$ and $\dot{\underline{e}}_C$, defined by:

$$\dot{\underline{e}}_{A,B,C} = \underset{\sim}{\omega} \times \underline{e}_{A,B,C} \qquad (4.1)$$

where ω is the molecular angular velocity. The vector a.c.f. $\langle \underline{e}_A(t).\underline{e}_A(o) \rangle$ is related by direct Fourier transform to the far infra-red power absorption coefficient ($\alpha(\bar{\nu})$ in neper cm^{-1}). The spectrum $\alpha(\bar{\nu})$ is a sensitive test of the theory of rotational diffusion in molecular liquids.

Having obtained by simulation the autocorrelation functions, $\langle \underline{e}_A(t).\underline{e}_A(o) \rangle$, $\langle \underline{e}_B(t).\underline{e}_B(o) \rangle$ and $\langle \underline{e}_C(t).\underline{e}_C(o) \rangle$, with areas τ_1, τ_2 and τ_3 respectively, the friction coefficients β_1, β_2 and β_3 of the phenomenological theory [1-3] may be estimated straightforwardly as follows

$$\begin{aligned} \tau_1^{-1} &= D_2 + D_3 \\ \tau_2^{-1} &= D_1 + D_3 \\ \tau_3^{-1} &= D_1 + D_2 \end{aligned} \qquad (4.2)$$

where $D_i = \dfrac{kT}{I_i \beta_i}$

Knowing β_1, β_2 and β_3 we can then aim to reproduce a range of computer simulation curves theoretically without recourse to any fitting procedure and with no free parameters.

Algorithm TETRA

This algorithm was originally written by Singer and coworkers. Ferrario modified it to include a charge-charge interaction and a force cut off criterion based on molecule centre of mass to centre of mass distance (cut off radius = 11.28Å). The equations of motion are solved with a third order predictor algorithm, which coincides with the two step Verlet algorithm as far as the translational motion of the centre of mass is concerned. Rotation is integrated using as coordinates the angular momentum and the three unit vectors along the principal axes.

The Lennard Jones parameters are as follows:

σ (H - H) = 2.75Å; σ (Cl - Cl) = 3.35Å;

σ (C - C) = 3.20Å; ε/k(H - H) = 13.4K;

ε/k (Cl - Cl) = 175.0K; ε/k (C - C) = 51.0K.

with fractional charges (when incorporated) of +0.098 e on H; -0.109 e on Cl; and +0.022 e on C. (e = absolute value of the electron charge).

The former were chosen to optimise the thermodynamic conditions and the latter from a molecular orbital calculation by del Re [8]. The molecules were initially set up on a face-centred lattice which melted over about 2000 time steps of 0.005 ps each. The main run was carried out at V = 64 cm^3 $mole^{-1}$ in about twelve sections each lasting 10 mins CPU of CDC 7600 time, (a total of about 7000 time steps). The dynamical data were collected every 5 steps, stored on 9 track magnetic tapes and analysed using a variety of programs designed primarily for the calculation of autocorrelation functions.

The 5 x 5 and 3 x 3 algorithms produce data which are directly comparable because the thermodynamic conditions are the same (293K, 1 bar, V = 64.0 cm^3/mole). Any difference in the resulting dynamical functions may therefore be attributed directly to the difference in the pairwise-additive force fields used. The results are also directly comparable with spectroscopic data over the range from zero to the THz frequencies (into the far infra-red), and results from the many related techniques now becoming available [2,3].

Description of Reduced Units: TRI2

The units of the dynamical quantities in the MKS system are related to the normalised units in TR12 as follows. If we use the symbol ^ to indicate quantities in the algorithm, then:

i) $\hat{\underset{\sim}{r}} = \underset{\sim}{r}/H$, where r is length in metres and H half the box length;

ii) $\hat{\varepsilon} = \varepsilon/H^2$, where ε is the Lennard-Jones energy factor;

iii) $\hat{\underline{F}} = \underline{F}/H$ where $\underline{F}$ is the resultant force on the molecule;

iv) $\hat{\underset{\sim}{T}} = \underset{\sim}{T}_q/H^2$, where $\underset{\sim}{T}_q$ is the resultant torque;

v) $\hat{\underset{\sim}{J}} = \underset{\sim}{J}/H^2$, where $\underset{\sim}{J}$ is the resultant angular momentum;

vi) $\hat{\underset{\sim}{e}}_{A,B,C} = \underset{\sim}{e}_{A,B,C}$, unit vectors in the axes of $\hat{I}_{A,B,C}$. The vector in the axis bisecting ABA is $\underset{\sim}{e}_A$;

vii) $\hat{\underset{\sim}{\omega}} = \underset{\sim}{\omega}$, the angular velocity;

viii) $\hat{I} = I/H^2$ where I is a moment of intertia;

ix) $\hat{\underset{\sim}{v}} = \underset{\sim}{v}(t/H)$ where t is the time-step in seconds. In the algorithm $\hat{\underset{\sim}{v}}$ is in box units per time-step.

The units in TETRA are effectively MKS normalised by the box length.

SECTION 2. MD SIMULATION RESULTS

TETRA: Equilibrium Results

Instantaneous values of thermodynamical quantities are recorded in TETRA and average values on the complete equilibrium run are available. Values of pressure and specific heat have been calculated according to the expressions given by Cheung [8].

Result without charges (3600 time steps).

{T = temperature (^{o}K); P = pressure (bar); U = internal energy (KJ/mole); E_T = total energy (trans. + rot.) (kJ/mole); C_V = specific heat at constant vol. in J $mole^{-1}K^{-1}$}.

<T> = 292.7 ± 9.2K (49.5% translational and 50.5% rotational).

<P> = 283 ± 312 bar

<U> = -23.69 kJ $mole^{-1}$

$\langle E_T \rangle$ = -(16.39 ± 0.21)kJ $mole^{-1}$

$\langle C_V \rangle$ = 37 J $mole^{-1}K^{-1}$, compared with 90 J $mole^{-1}K^{-1}$ experimentally [5].

This is of course a fluctuation property ($\Delta U/\Delta T$) and ideally needs runs upwards of 20,000 steps for good statistics.

Results with Charges

<T> = 294.5 ± 11.0 K (50.2% translational, 49.8% rotational)

<P> = 273 ± 300 bar

<U> = -25.46 kJ $mole^{-1}$

(-6.1 kcal $mole^{-1}$)

$\langle E_T \rangle$ = -(18.11 ± 0.13) kJ $mole^{-1}$

$\langle C_V \rangle$ = 46.0 J $mole^{-1}K^{-1}$.

The total and potential energy is significantly affected by the inclusion of charges in the algorithm and so also are the atom-atom pair distribution functions.

Atom-Atom Pair Distribution Functions

There are available with and without charges from the 5 x 5 algorithm TETRA. They measure essentially the probability of finding another atom (A) at a distance $\underset{\sim}{r}$ (A) from a given atom (B) on another molecule at thermodynamic equilibrium. If the p.d.f. is structured with two or three peaks then this implies that the liquid as a whole also has a fair degree of residual ordering in comparison with the crystalline lattice. Fig. (1) illustrates the situation, for example in the p.d.f. describing H —— H atom-atom positions. It is by no means certain that the structure can be attributed solely to repulsive parts of the intermolecular potential (as in RISM theory) because the addition of charges clearly inhibits the first peak at about 2.8Å while enhancing the second. Neutron and X-ray diffraction measurements on isotopically substituted CH_2Cl_2 should provide an

experimental test of the simulation and improve thereby our knowledge of the intermolecular potential. Similarly, Figs. (2) to (6) reflect this sensitivity of p.d.f. structure to electrodynamic parts of the pair potential. For example, the first peak in the H —— Cl p.d.f. is enhanced; that for H —— C inhibited, the

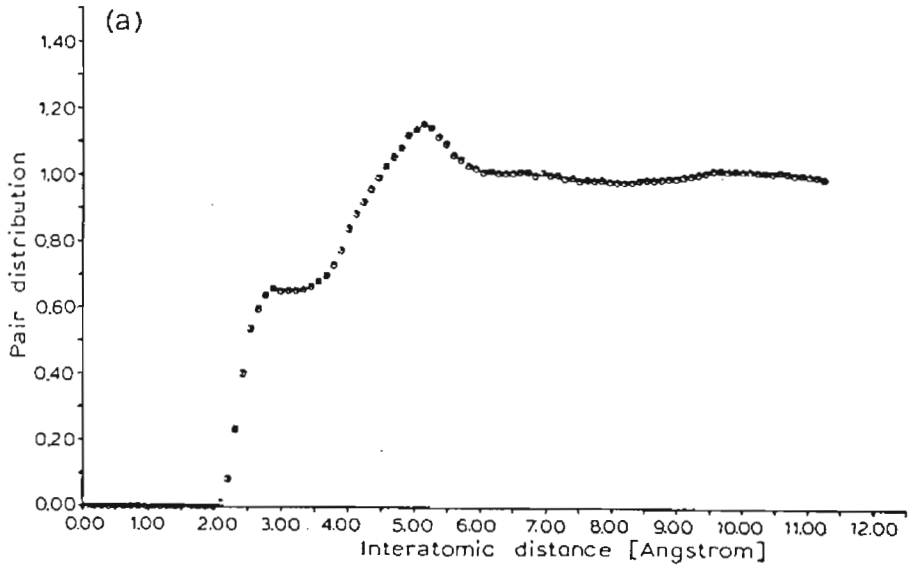

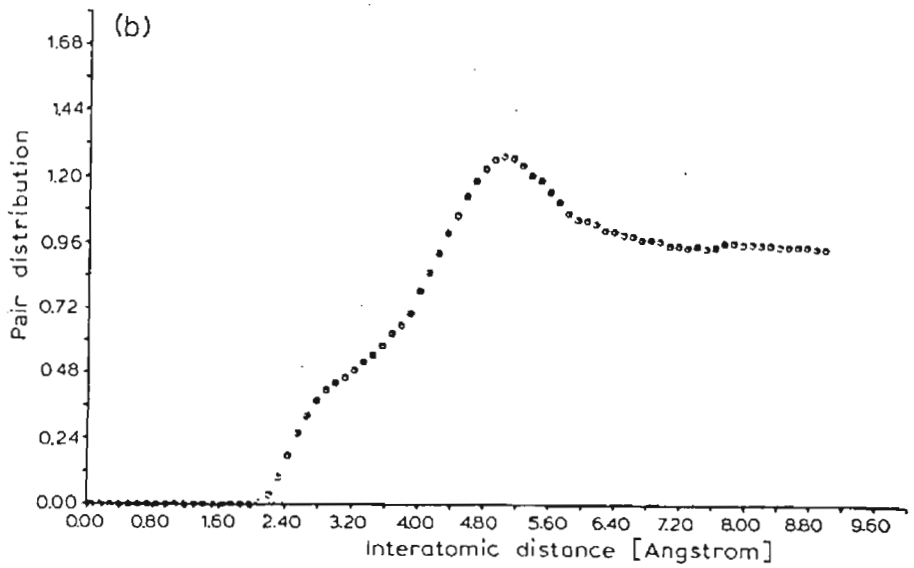

Figure Captions

Figure (1)

a) Hydrogen to hydrogen atom-atom pair distribution function extracted as a mean over the equilibrium run. 5 x 5 potential, no charges. 293K, 1 bar.

b) Plus charges.

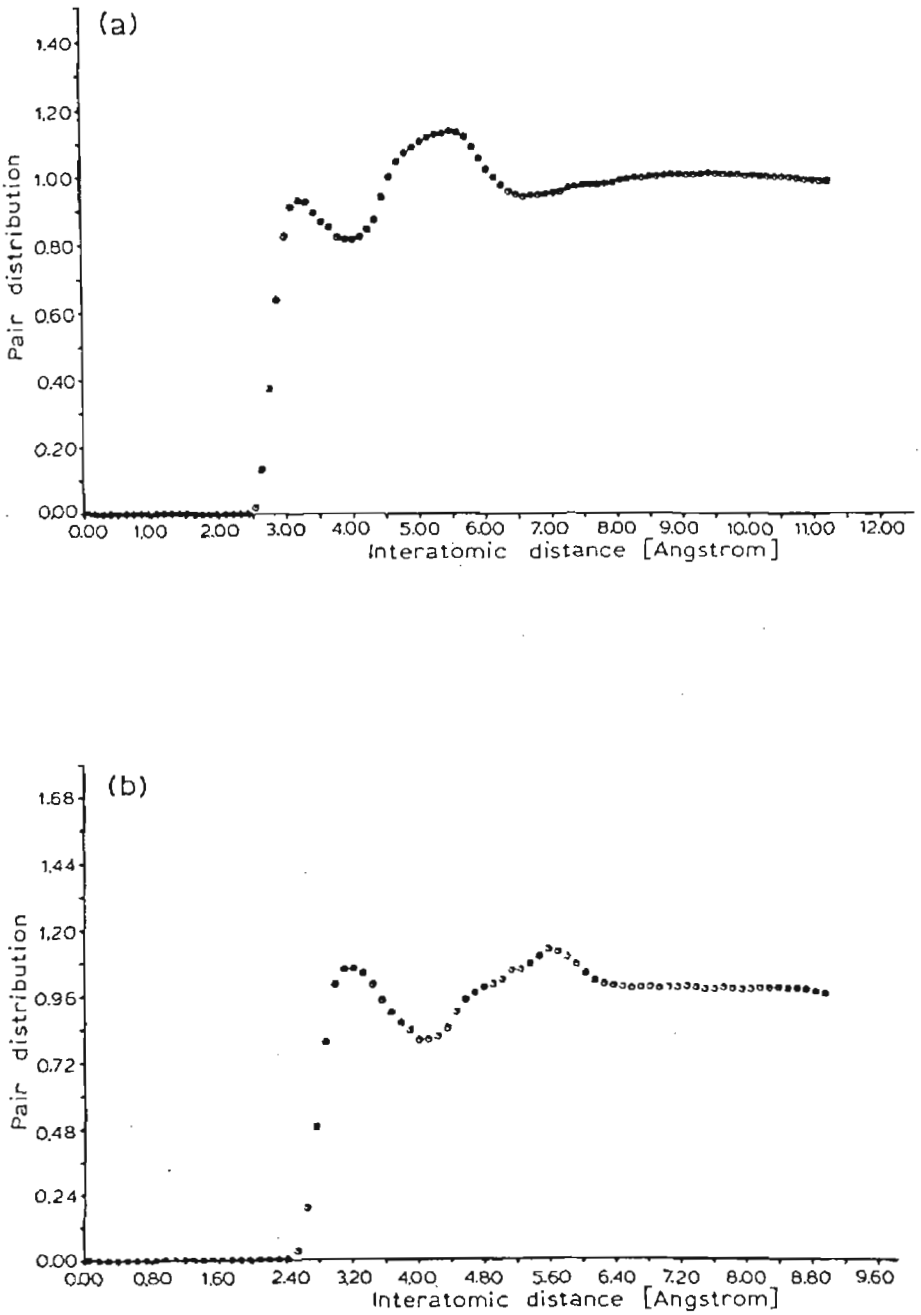

Figure (2)

As for Fig. (1), hydrogen to chlorine.

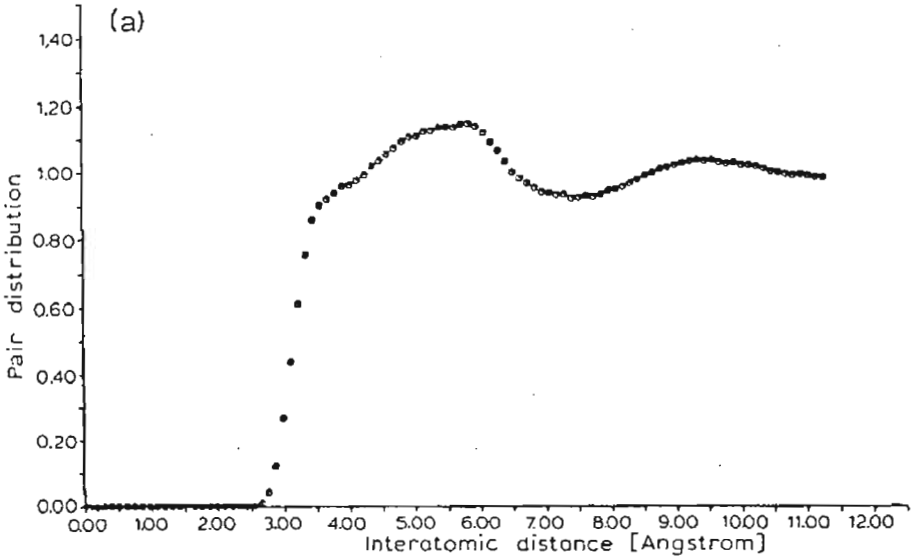

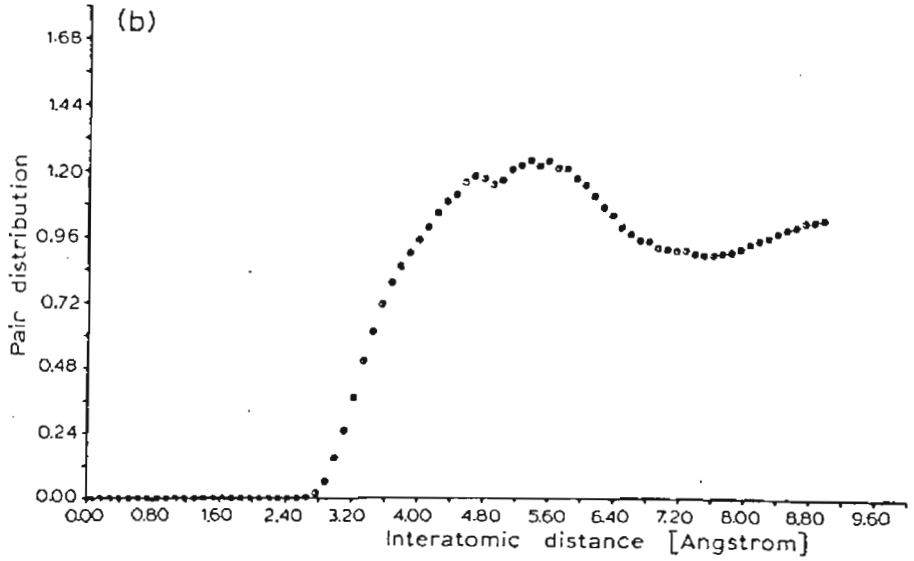

Figure (3)

As for Fig. (1), hydrogen to carbon.

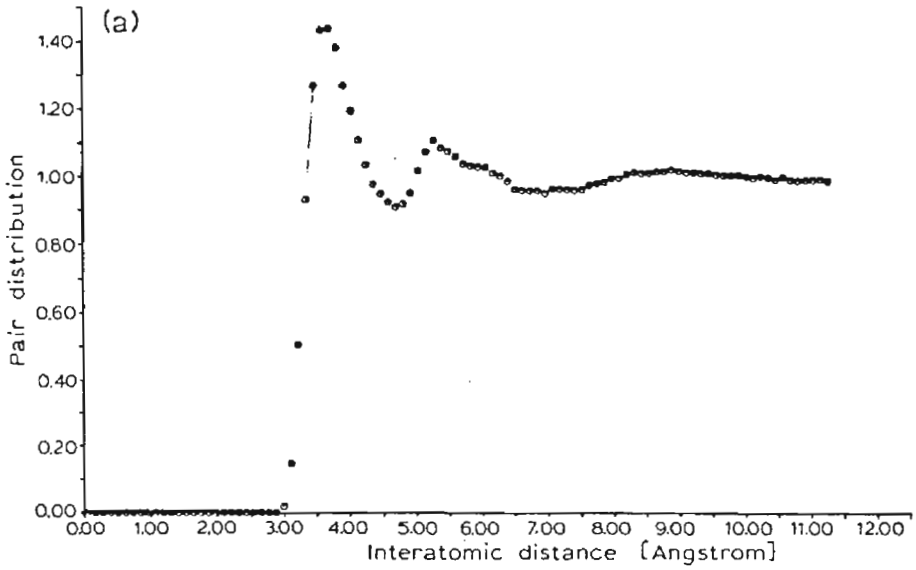

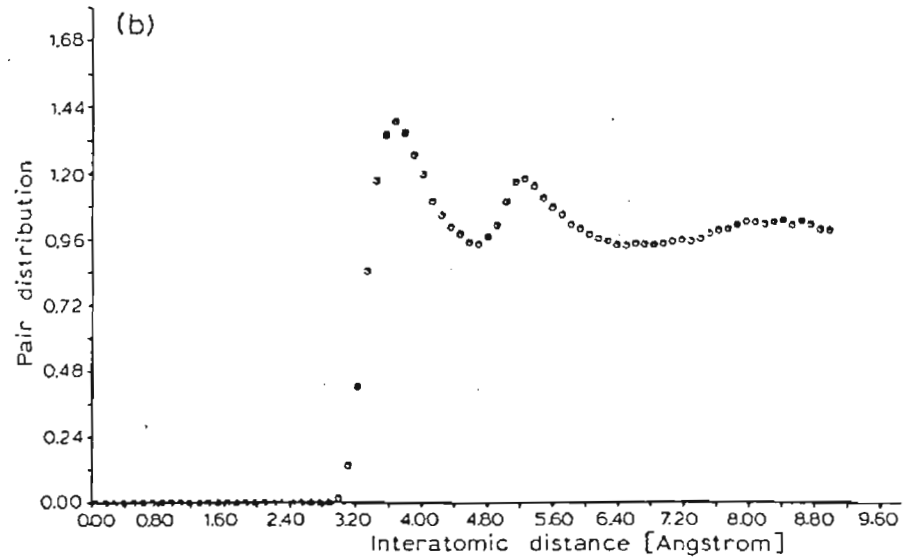

Figure (4)

As for Fig. (1), chlorine to chlorine.

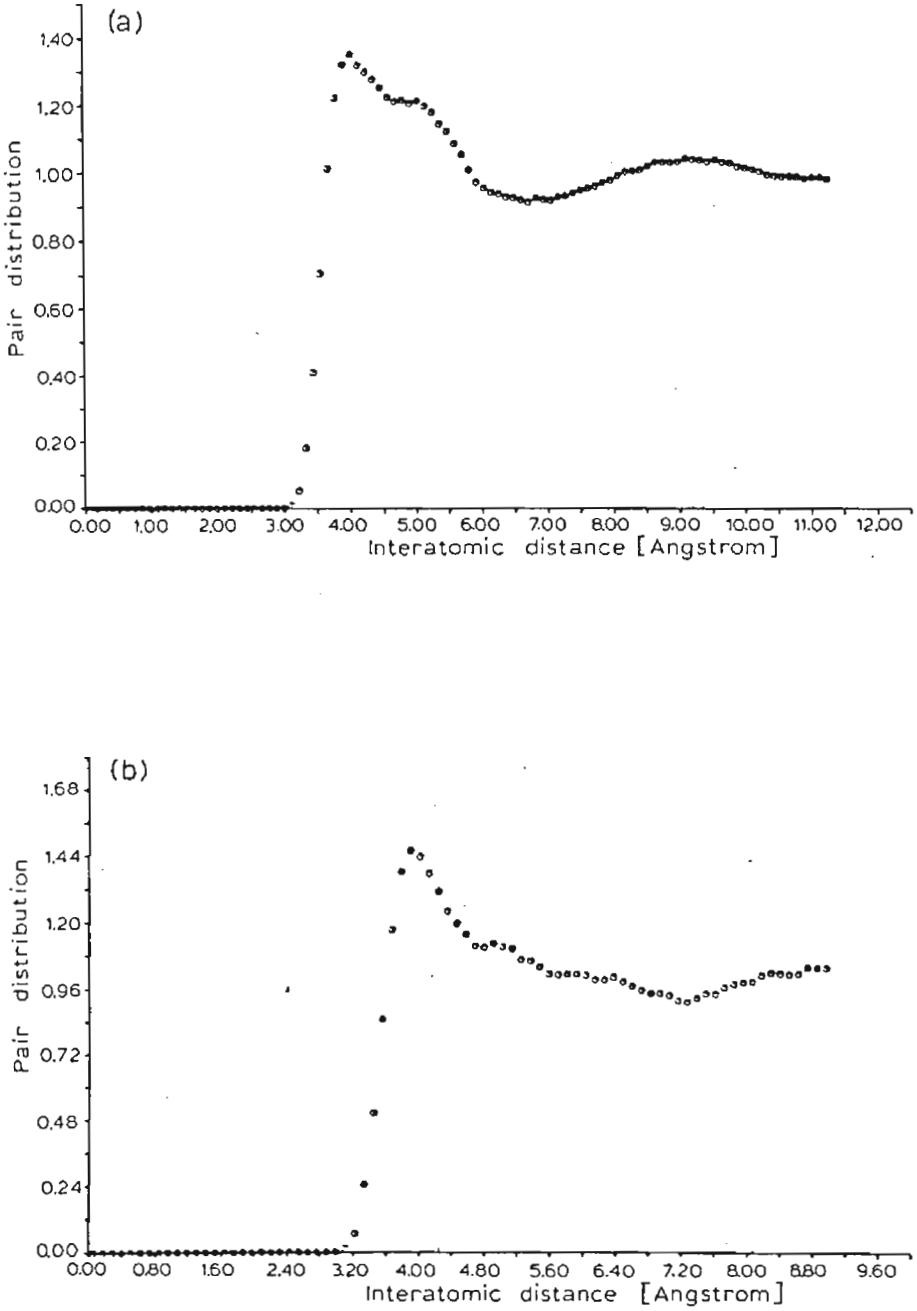

Figure (5)

As for Fig. (1), chlorine to carbon.

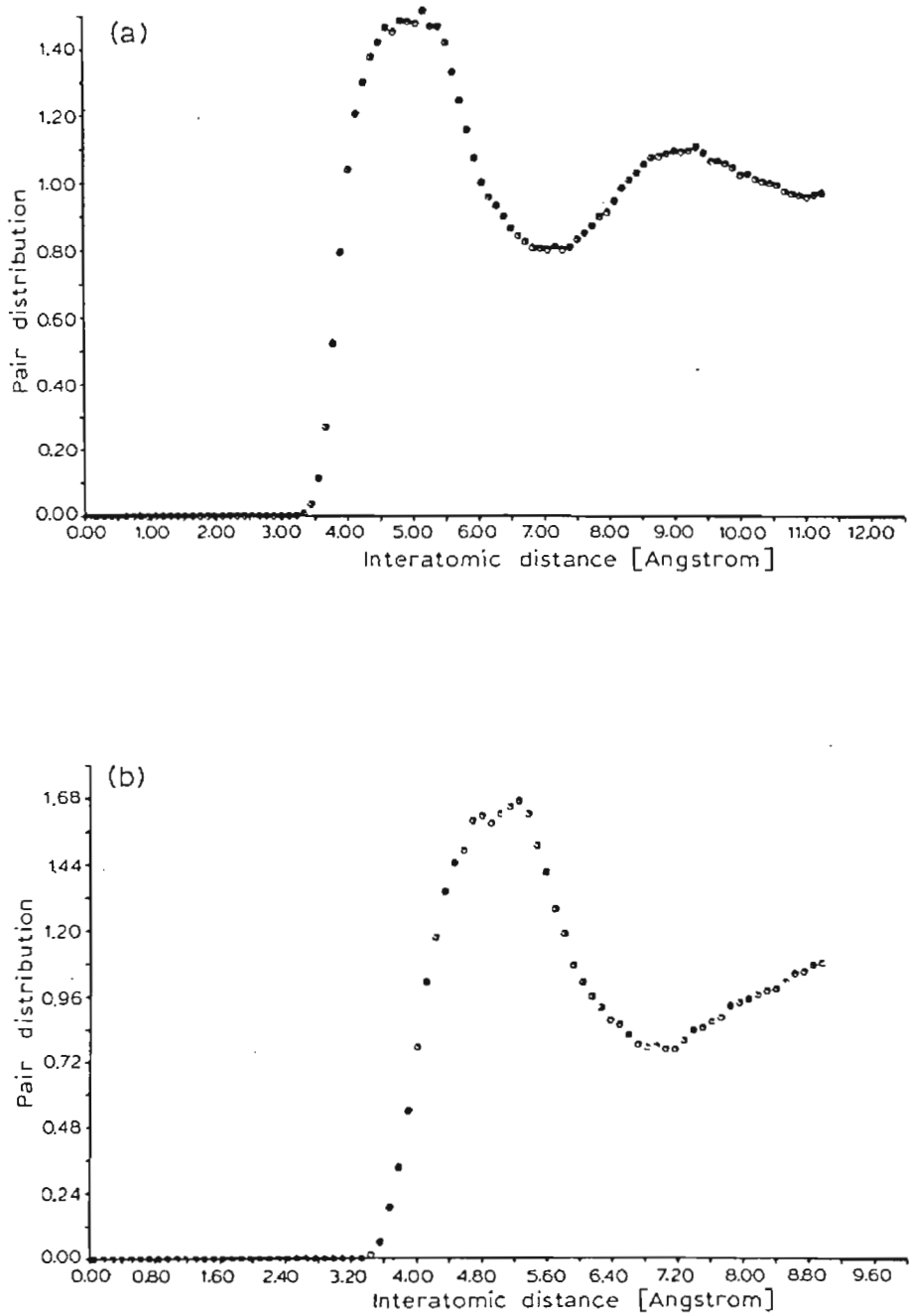

Figure (6)

As for Fig. (1), carbon to carbon.

second peak in Cl —— Cl is sharpened; the shoulder in Cl —— C is decreased; and the main peak in C —— C slightly sharpened.

Dynamical Results

A discriminating test of either simulation is the observed far infra-red power absorption coefficient 2,3 and in Fig. [7] we plot a comparison. Although the simulated spectrum are affected by artifacts introduced by the numerical Fourier transform of $\langle \dot{\underline{e}}_A(t).\dot{\underline{e}}_A(o)\rangle$ it is clear that the 5 x 5 algorithm is the more realistic in comparison with the observed data. We note that the simulated curve (1) has been derived from an auto-correlation function, and secondly the intensity of the simulated spectra was estimated using the observed static dielectric permittity for pure liquid CH_2Cl_2 of ε_o = 9.02 with a Fatuzzo-Mason internal field correction. By Fourier transforming $\langle \dot{\underline{e}}_A(o).\Sigma_{i=1}^{N} \dot{\underline{e}}_{Ai}(t)\rangle$ we obtain the spectrum from the result of fig. (34). This cross or microscopic

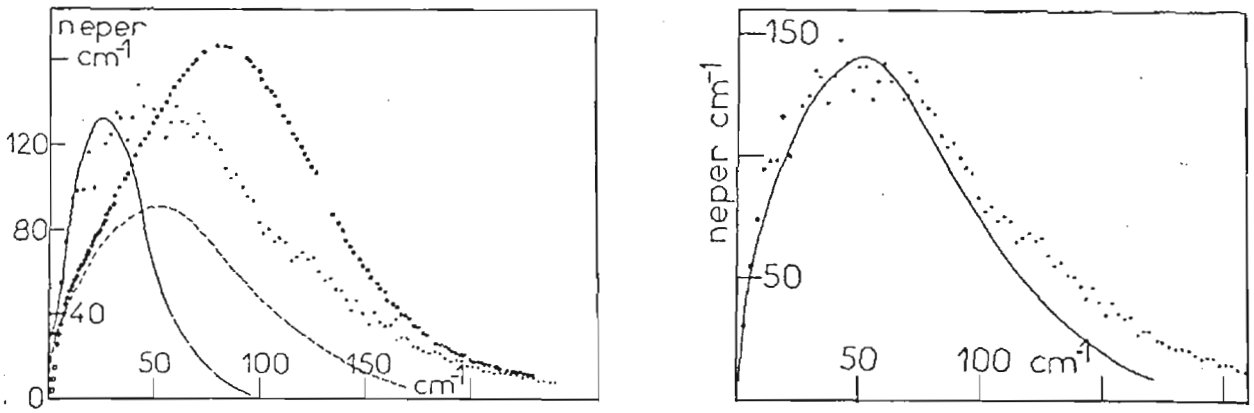

Figure (7)

Comparison of molecular dynamics simulation and far infra-red spectra of CH_2Cl_2 and solution in CCl_4.

o
⟡ } Measured data (interferometers and klystrons)
□

• Computer simulation, 5 x 5 potential, no charges.

—— Computer simulation, 3 x 3 potential, no charges.

- - - 10% solution in CCl_4.

Figure (8)

Comparison of • simulation, and - - - - scaled up spectrum of CH_2Cl_2 in CCl_4, at 293K.

correlation function was computed using a sphere of 8Å radius.

In fig. (8) we have plotted the numerical Fourier transformation of $\langle \dot{\underline{e}}_A(t).\dot{\underline{e}}_A(o)\rangle$ from the 5 x 5 algorithm without charge interactions directly on to the spectrum of 10% CH_2Cl_2 in dilute decalin taken by Reid and Evans[2]. The two curves have been normalised for clarity and it seems to be significant that the match is very good except in the high frequency wing where the simulated spectrum decays more slowly. Furthermore the microwave correlation time measured by Reid for CH_2Cl_2 in 10% decalin solution is 1.2 $\pm$ 0.3 ps, and the area beneath the simulated correlation $\langle \underline{e}_A(t).\underline{e}_A(o)\rangle$ is also 1.2ps. From these results we may suppose:

i) that the hydrogen atoms play an important part in the dynamics of CH_2Cl_2.

ii) Fig. (8) is a comparison of a computer simulation of neat CH_2Cl_2 liquid leaving out the electrodynamical (charge-charge) interactions with an experimentally observed spectrum of CH_2Cl_2 in dilute decalin solution. The electrodynamics in the latter case seem therefore to have been isolated effectively from the kinematics. In other words in dilute CH_2Cl_2/decalin solution we may suppose that we are looking at the auto-correlation function of CH_2Cl_2 with negligible multipole-multipole interaction, or cross correlation.

iii) The similarity of band-shape in Fig. (8) suggests that induced absorption effects are minimal in affecting the spectrum of CH_2Cl_2 in dilute decalin solution. To corroborate these results we need experimental spectra of still higher quality.

The usual Legendre (orientational) auto-correlation functions P_1 and P_2 are illustrated in Figs. (9) respectively for the vectors $\underline{e}_A$, $\underline{e}_B$ and $\underline{e}_C$ of the 5 x 5 algorithm. The fall-off of the a.c.f.'s of $\underline{e}_A$ and $\underline{e}_C$ is similar in both cases, while that of $\underline{e}_B$ is much slower. The areas of the curves in Fig.(9b) can be related straightforwardly to N.M.R. correlation times in CH_2Cl_2 (using reasonances of C, Cl, H and D). However, Brier and Perry[1] have shown that the available experimental times in this case are unreliable and ideally should be carefully remeasured at 293 K, 1 bar for the purpose of direct comparison.

In Fig. (10a) we plot P_1 and P_4 for the $\underline{e}_A$ vector from 3 x 3 algorithm and compare these with P_1 from the 5 x 5 algorithm. It is clear that the 3 x 3 algorithm produces non-exponential a.c.f.'s which decay too quickly even in comparison with experimental data on CH_2Cl_2 in dilute decalin solution. Bearing this in mind it is nevertheless quite interesting to look at the difference between Figs. (10a) and (10b). In the latter we have simulated P_1 to P_4 for $\underline{e}_A$, $\underline{e}_B$ and $\underline{e}_C$ from the 3 x 3 algorithm at 5000 bar, 323 K, (another pilot project

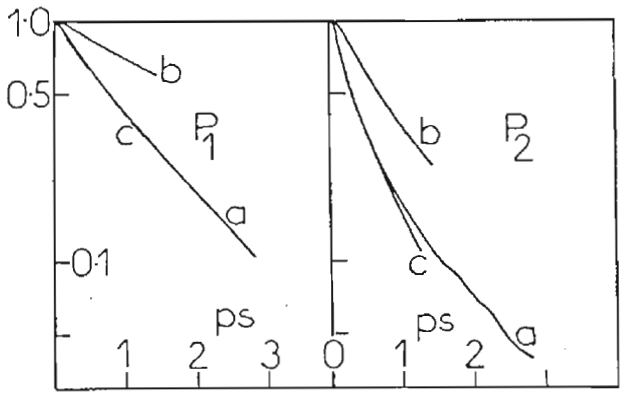

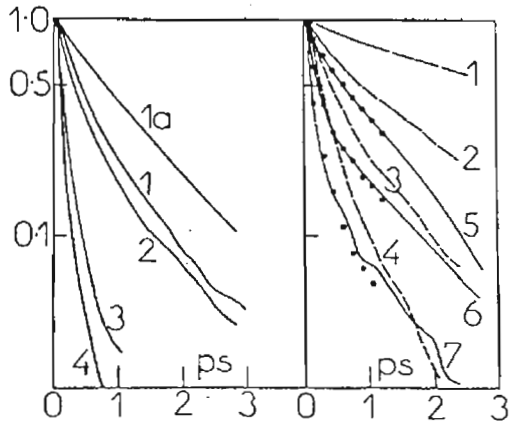

Figure (9a)

5 x 5 potential, no charges. P_1 orientational a.c.f. of: a) the dipole unit vector ($\underline{e}_A$); b) the orthogonal vector $\underline{e}_B$; c) the mutually orthogonal vector $\underline{e}_C$.

Figure (9b)

As for Fig. (3), P_2 (N.M.R.) a.c.f.'s.

Figure (10a)

Curves (1) to (4), P_1 to P_4 a.c.f.'s of $\underline{e}_A$, 3 x 3 potential, no charges. For comparison, curve 1a is the P_1 a.c.f. of $\underline{e}_A$ from the 5 x 5 potential, no charges.

Figure (10b)

3 x 3 potential, no charges, at 5 kbar, 323K. Curves (1) to (4): P_1 to P_4 a.c.f. of $\underline{e}_B$. Curves (5) to (7): P_1 to P_3 a.c.f.'s of $\underline{e}_A$; ⊙ of $\underline{e}_C$.

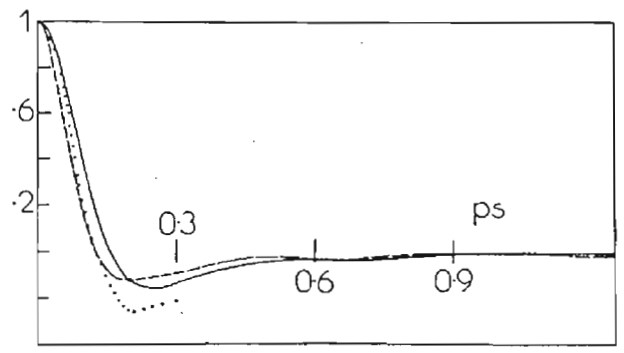

Figure (11)

Rotational velocity a.c.f.'s (of $\dot{\underline{e}}_A(t)$).

——— 3 x 3 potential, no charges;

- - - 5 x 5 potential, no charges;

..... for 10% (v/v) CH_2Cl_2 in CCl_4.

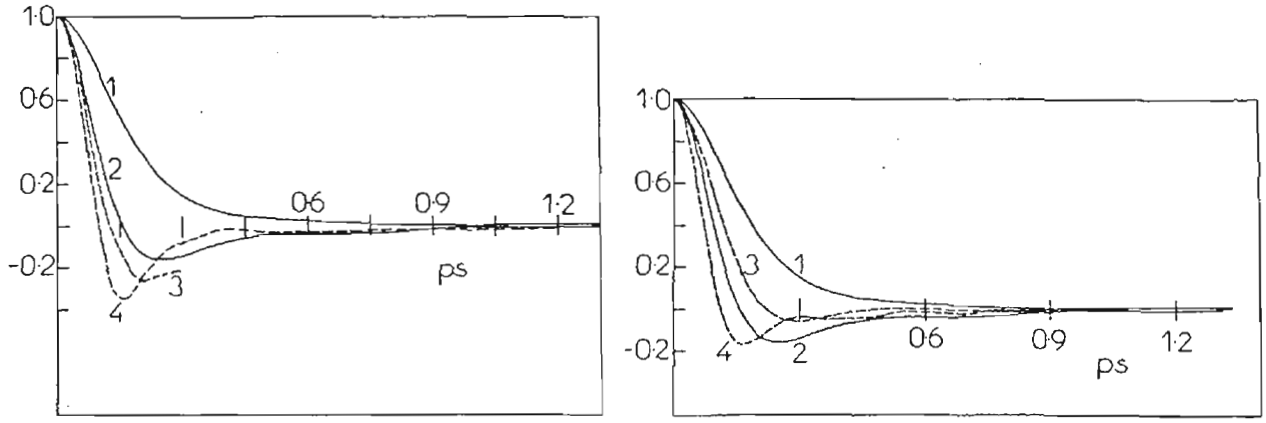

Figure (12)

Comparison of (1) angular momentum a.c.f. with (2) the a.c.f. of $\underline{\dot{e}}_A(t)$ and (3) and (4) respectively the rotational velocity a.c.f.'s from CH_2Cl_2 data in solution and pure liquid state. Normalised as usual to 1 at t = o. 3 x 3 potential, no charges.

Figure (13)

(1) and (2) Angular momentum and $\underline{\dot{e}}_A(t)$ a.c.f.'s respectively at 293K, 1bar.

(3) and (4) at 5kbar, 323K.

3 x 3 potential, no charges.

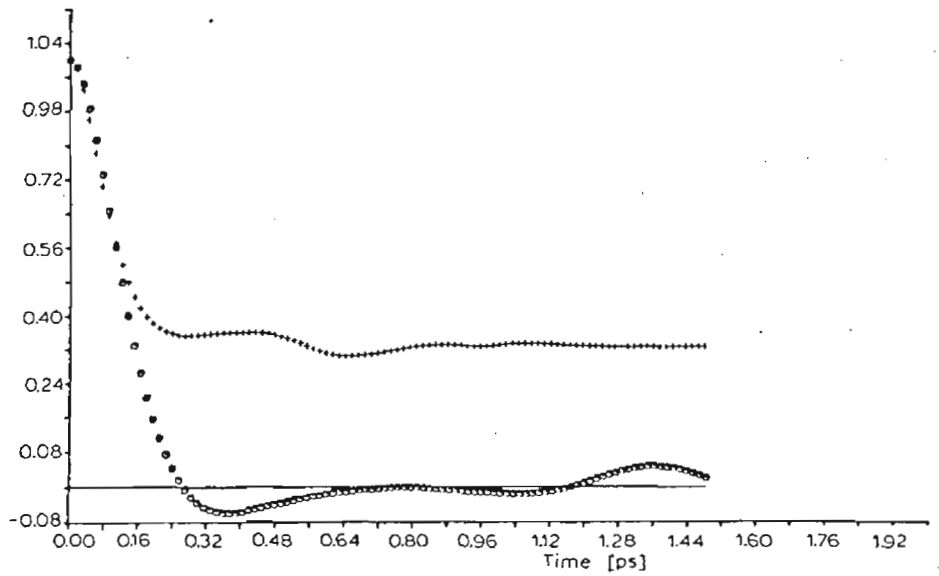

Figure (14)

TETRA algorithm = 5 x 5 atom-atom Lennard Jones plus electrostatic interaction. Angular momentum in the molecule fixed frame a.c.f.s.

Component $\underline{J}_1(\tau)$ parallel to the principal axis $\underline{e}_A$.

o $\langle \underline{J}_1(\tau).\underline{J}_1(o)\rangle / \langle \underline{J}_1^2(o)\rangle$

+ $\langle \underline{J}_1^2(t)\ \underline{J}_1^2(o)\rangle / \langle \underline{J}_1^4(o)\rangle$

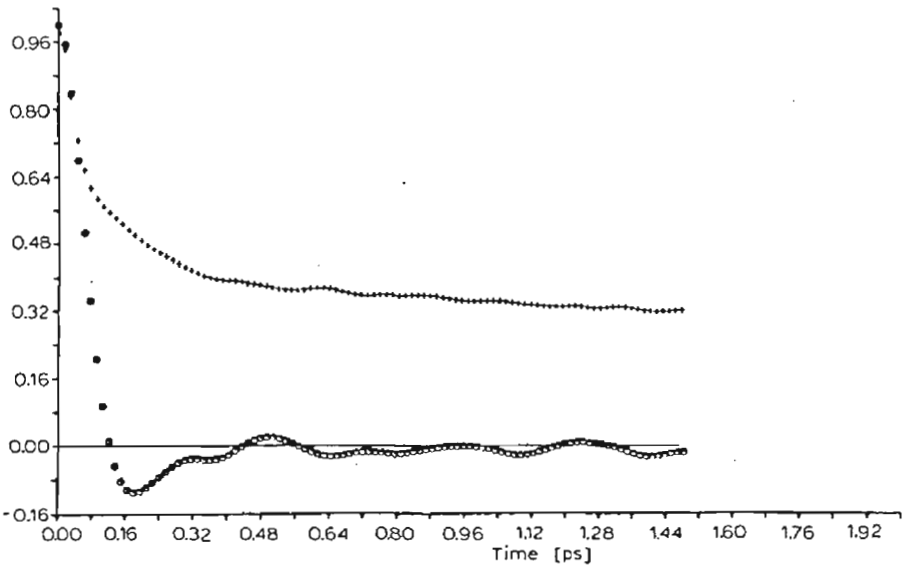

Figure (15)

As for Fig. (14). Component $\underline{J}_2(\tau)$ parallel to the $\underline{e}_B$ principal axis.

state point of EMLG). Relative to those in Fig. (10a), the a.c.f.'s in Fig. (10b) decay more slowly, and the anisotropy between $\underline{e}_B$ and $\underline{e}_C$ has increased. This gives us an indication of what should be observable experimentally if the techniques ever become available for the measurement of P_1 to P_4 under hydraulic pressure. When the anisotropy of rotational diffusion reaches a certain point the liquid will of course solidify through the application of pressure.

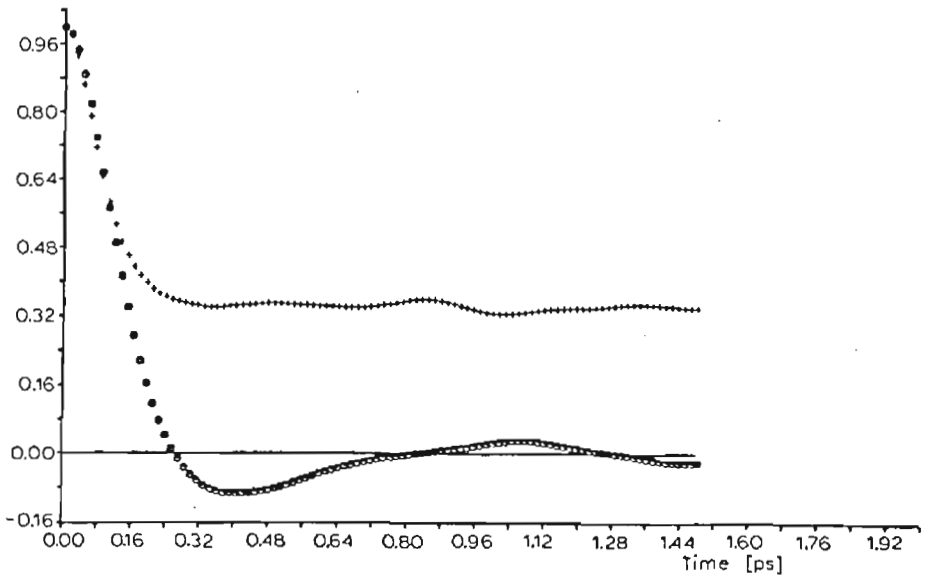

Figure (16)

As for Fig. (14). Component $\underline{J}_3(\tau)$ parallel to the $\underline{e}_C$ principal axis.

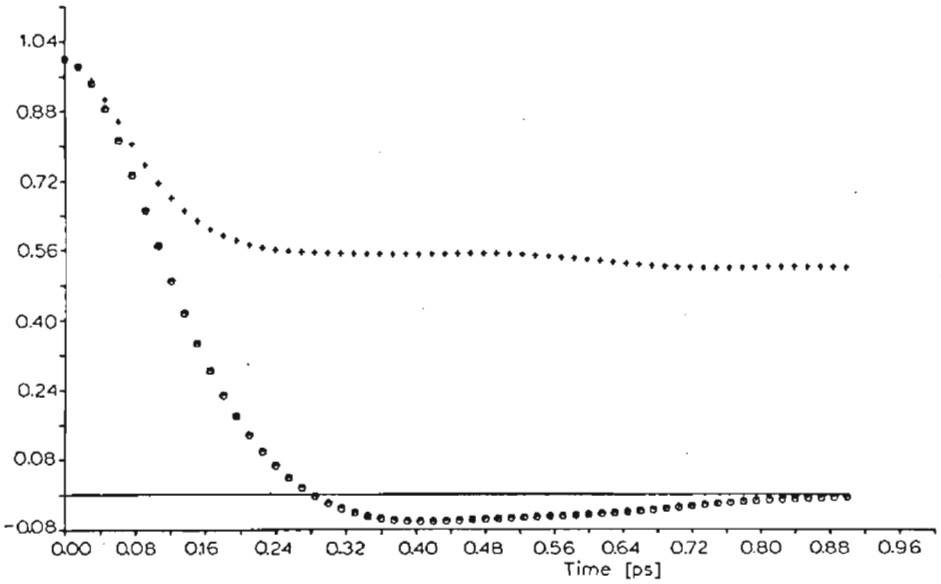

Figure (17)

Tetra algorithm, as for Fig. (14). Angular momentum $\underline{J}(\tau)$ in the lab. frame a.c.f.s.

o $\langle \underline{J}(\tau).\underline{J}(o)\rangle / \langle \underline{J}^2(o)\rangle$

+ $\langle \underline{J}^2(\tau)\ \underline{J}^2(o)\rangle / \langle \underline{J}^4(o)\rangle$

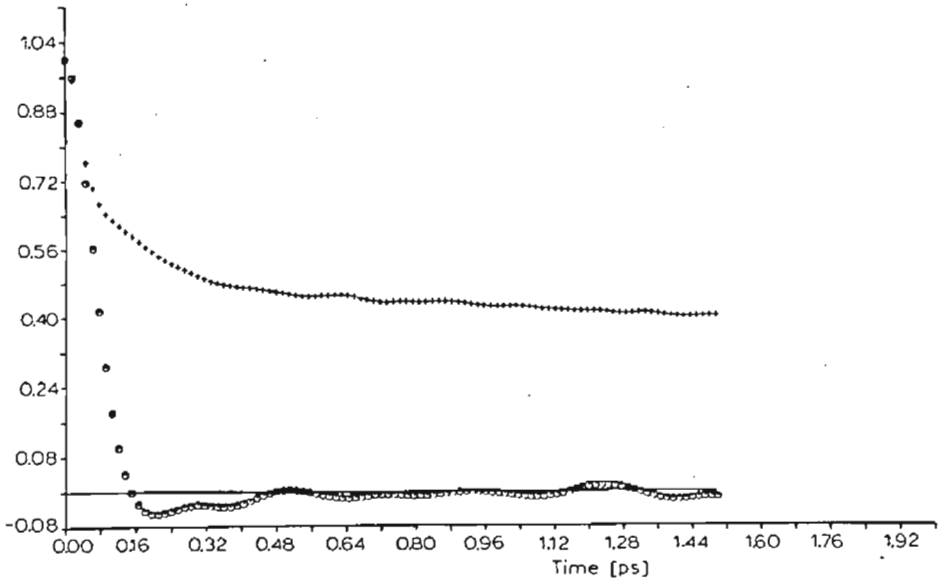

Figure (18)

Tetra algorithm, as for Fig. (14) - Angular velocity $\omega(\tau)$ in the laboratory frame, a.c.f.s.

o $\langle \underline{\omega}(\tau).\underline{\omega}(o)\ \rangle / \langle \omega^2(o)\rangle$

+ $\langle \omega^2(\tau)\ \omega^2(o)\rangle / \langle \omega^4(o)\rangle$

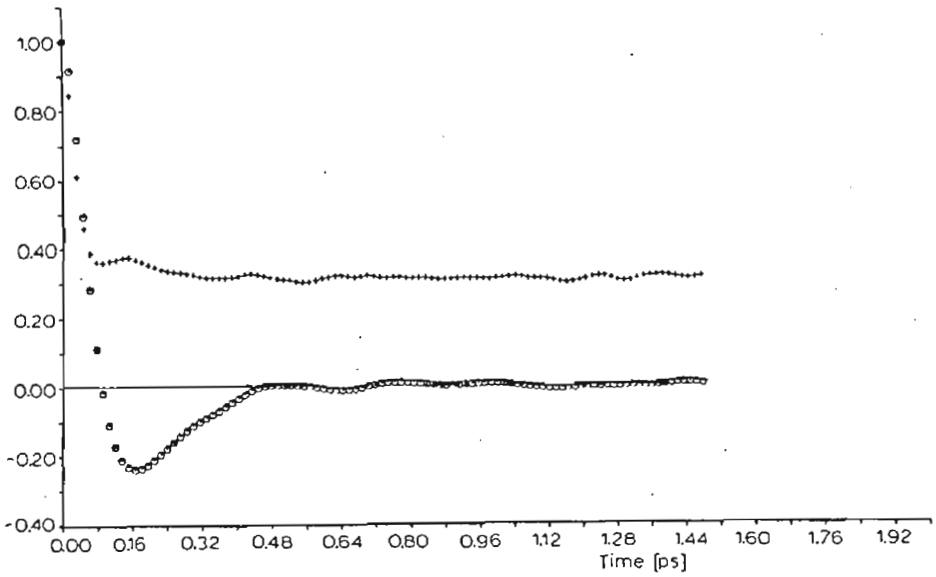

Figure (19)

Tetra algorithm, as for Fig. (14) - Torque $\underline{N}(\tau)$ in the lab. frame, a.c.f.s.

o $\langle \underline{N}(\tau).\underline{N}(o)\rangle / N^2(o)$

+ $\langle N^2(\tau)N^2(o)\rangle / \langle N^4(o)\rangle$

Fig. (11) illustrates the a.c.f. $\langle \dot{\underline{e}}_A(t).\dot{\underline{e}}_A(o)\rangle$ from both the 5 x 5 and 3 x 3 algorithms in comparison with the Fourier transform of the far infra-red power absorption coefficient for a 10% v/v solution of CH_2Cl_2 in decalin. The experimental curve is deeper and slightly more oscillatory. In Fig. (12) we illustrate the angular momentum auto-correlation function $\langle \underline{J}(t).\underline{J}(o)\rangle / \langle J^2(o)\rangle$ from the 3 x 3 algorithm in comparison with $\langle \dot{\underline{e}}_A(t).\dot{\underline{e}}_A(o)\rangle / \langle \dot{e}_A(o)\rangle$ computed under the same conditions (293K, 1 bar) and Fourier transforms of the far infra-red $\alpha(\bar{\nu})$ in dilute solution and in pure liquid. The angular momentum a.c.f. has a small but long positive tail and the rotational velocity a.c.f. a correspondingly long negative tail which makes it difficult to back Fourier transform numerically without introducing artifacts (Fig. (7)). There is a clear difference between the decay times of each function, which lessens (Fig. (13)) at 5000 bar, 323K. In Fig. (13) the functions are markedly more oscillatory and the simulated far infra-red spectrum is shifted to higher frequency.

It is interesting from a theoretical point of view to use the 5 x 5 algorithm to extract at 293K, 1 bar, angular velocity and angular momentum autocorrelation functions in both the laboratory and molecular frames (fixed by the principal moments of inertia axes labelled 1, 2 and 3 for $\underline{e}_A$, $\underline{e}_B$ and $\underline{e}_C$ respectively). The angular momentum a.c.f.'s in this molecule fixed frame are illustrated in Figs. (14)

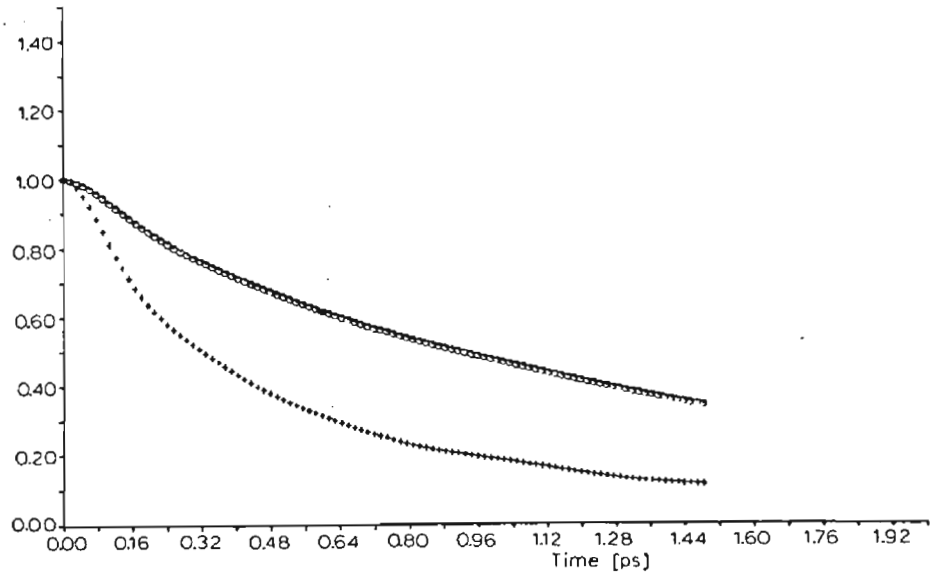

Figure (20)

Tetra algorithm, as for Fig. (14) - orientation a.c.f.s.

o $P_1(\underline{e}_A(\tau).\underline{e}_A(o)>$

+ $P_2(\underline{e}_A(\tau).\underline{e}_A(o)>$

to (16) together with the a.c.f.'s of the square values - the correlation time about the 2 principal-axis is the shortest, corresponding to smallest principal moment of inertia. It is possible to note that the $t\to\infty$ limit of the square values a.c.f.'s is about $^1/3$ corresponding to gaussian equilibrium statistics. The transient behaviour of this a.c.f. is not Gaussian. The angular momentum in the lab-frame - acf and its square value a.c.f. $<J^2(t)\ J^2(o)>/<J^4(o)>$ are shown in fig. (17). The angular velocity a.c.f.'s are illustrated for comparison in fig. (18). The torque and its square value a.c.f.'s show deeper oscillation (fig. (19)).

Finally in this section the orientational autocorrelation functions from the 5 x 5 molecular dynamics simulation are described in Figs. (20) to (22). Figs. (20) and (22) illustrate P_1 and P_2 for the dipole vector and the one related to the biggest principal moment of inertia. The latter correlation time, Fig. (21), is considerably the longer, as in the 3 x 3 case. The theoretical model reproduces the simulation data very closely. Figs. (23) illustrate the rotational velocity a.c.f. for the unit vector $\underline{e}_A$, $<\dot{\underline{e}}_A(t).\dot{\underline{e}}_A(o)>/<\dot{\underline{e}}_A(o).\dot{\underline{e}}_A(o)>$, parallel to the dipole vector. This is oscillatory with a long, negative tail.

In the foregoing we have concentrated on reorientational, angular momentum and torque a.c.f.'s but a complete description of liquid phase dynamics involves

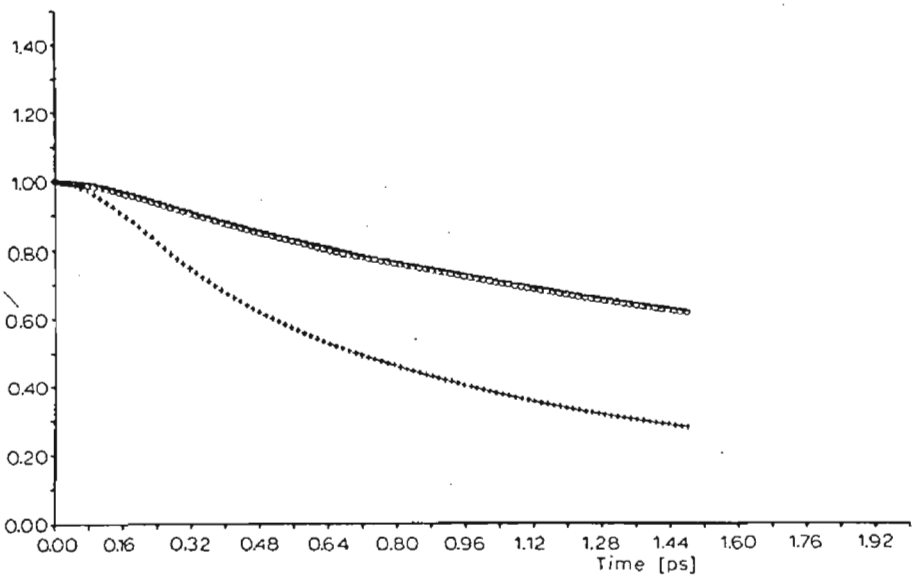

Figure (21)

As for Fig. (20)

o $P_1(\underline{e}_B(\tau).\underline{e}_B(o))$

\+ $P_2(\underline{e}_B(\tau).\underline{e}_B(o))$

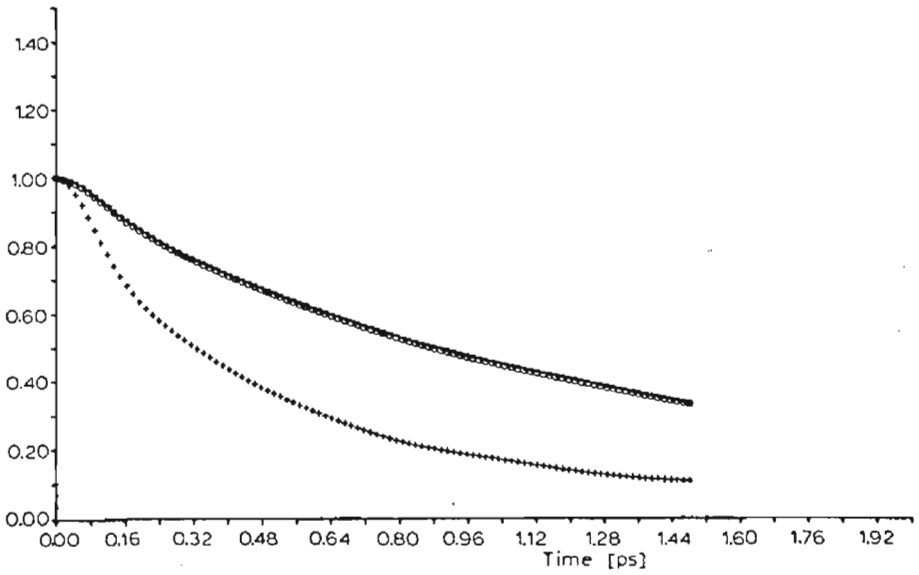

Figure (22)

As for Fig. (20)

o $P_1(\underline{e}_C(\tau).e_C(o))$

\+ $P_2(\underline{e}_C(t).e_C(o))$

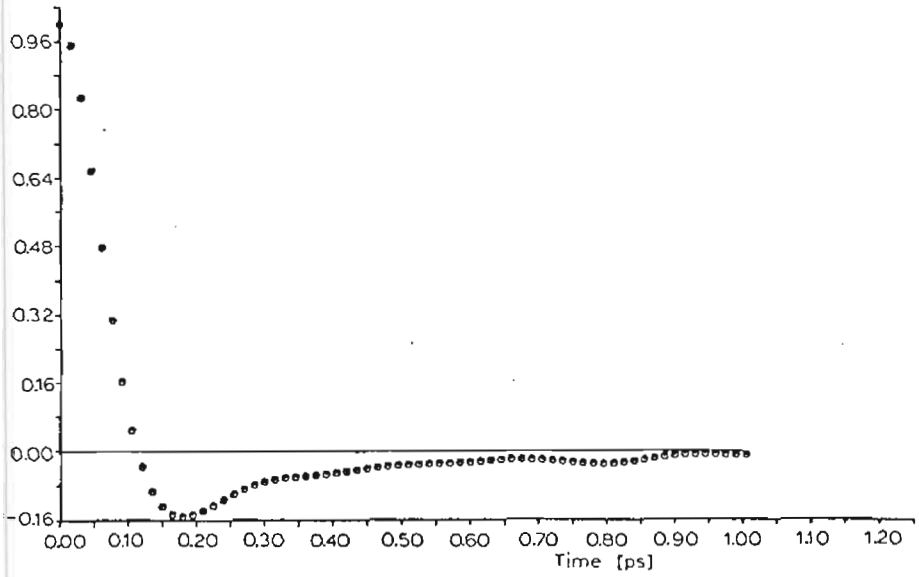

Figure (23)

Tetra Algorithm, as for Fig. (14). Rotational velocity a.c.f.
$\langle \dot{e}_A(\tau).\dot{e}_A(o)\rangle / \langle \dot{e}_A^2(o)\rangle$

in addition a consideration of centre of mass translation. The most straightforward autocorrelation function is that of the centre of mass velocity and kinetic energy (Fig. (24)). For their theoretical description these need the use of theory based on the translational friction coefficient. This may be estimated from the area of the velocity a.c.f. of Fig. (24). Subsequently the phenomenological theory should produce the curves of Figs. (24) and (25) dealing with the velocity, energy, force a.c.f., $\langle F^2(t)F^2(o)\rangle / \langle F^4(o)\rangle$. This last a.c.f. goes to a constant limit, determined by equilibrium statistics.

Having considered both the rotational and translational aspects of the 5 x 5 simulation results we turn finally to a calculation of mixed autocorrelation functions. There is no clear cut experimental method yet developed to investigate these functions directly, but they can be simulated with little difficulty. The mixed a.c.f. $\langle \underset{\sim}{v}(o).\underset{\sim}{J}(t)\rangle$ vanishes for all t because the parity of $\underset{\sim}{v}$ is different from $\underset{\sim}{J}$. Accordingly any attempt at simulating this function produces the background noise (Fig. (26)). (The application of a symmetry breaking external field may, however, produce a non-vanishing $\langle \underset{\sim}{v}(o).\underset{\sim}{J}(t)\rangle$.) The "mixed energy" a.c.f. $\langle v^2(o)J^2(t)\rangle / \langle v^2(o)\rangle\langle J^2(o)\rangle$ exists (Fig. 27). The 3 x 3 and 5 x 5 results in this case are fairly similar (Fig. (28)). Similar results are displayed for the mixed force/torque a.c.f.'s in Figs. (29) to (30). The a.c.f.'s $\frac{\langle N^2(o)F^2(t)\rangle}{\langle N^2(o)\rangle\langle F^2(o)\rangle}$ and $\frac{\langle F^2(o)N^2(t)\rangle}{\langle F\ (o)\rangle\langle N^2(o)\rangle}$ in particular are interesting in that the t = o values do <u>not</u> factorise. This means that $\langle F^2(o)N^2(o)\rangle \neq \langle F^2(o)\rangle\langle N^2(o)\rangle$ at t = o and there are strong rotation/translation effects (or "coupling") in these a.c.f.'s.

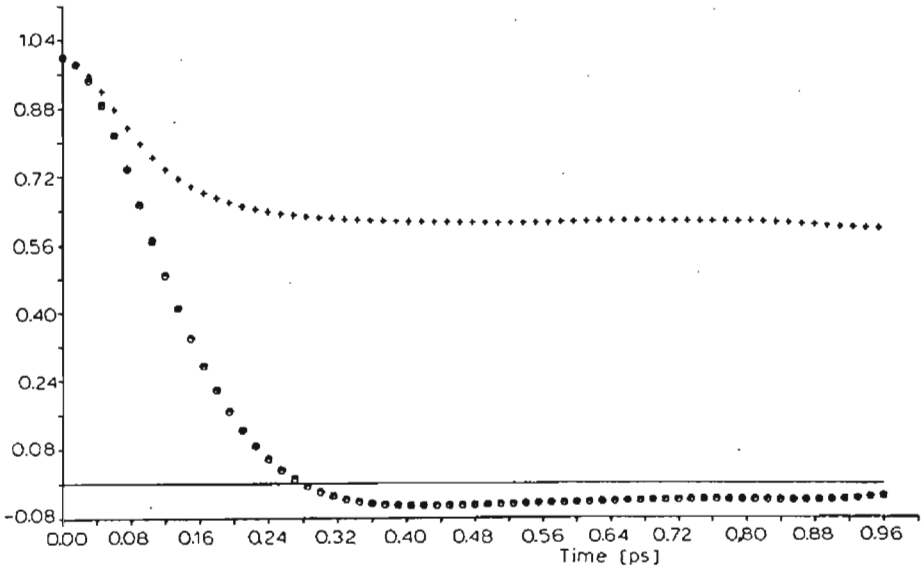

Figure (24)

Tetra algorithm, as for Fig. (14) - Center of mass velocity $\underline{V}(t)$ a.c.f.s.

o $\langle \underline{V}(t).\underline{V}(o)\rangle / \langle V^2(o)\rangle$

$\langle V^2(t).V^2(o)\rangle / \langle V^4(o)\rangle$

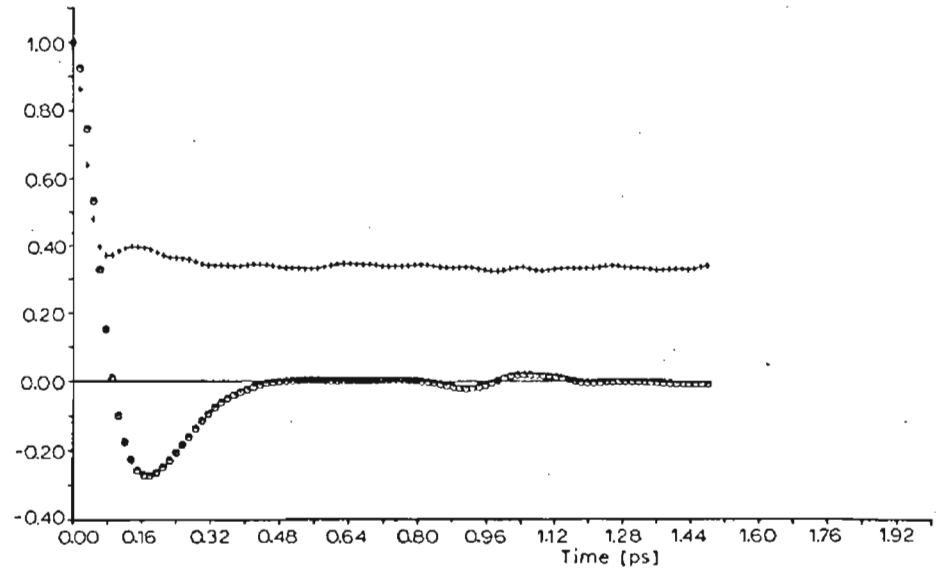

Figure (25)

Tetra algorithm, as for Fig. (14). Total force $\underline{F}(t)$ on each molecule, a.c.f.s.

o $\langle \underline{F}(t).\underline{F}(o)\rangle / \langle F^2(o)\rangle$

+ $\langle F^2(t)\ F^2(o)\rangle / \langle F^4(o)\rangle$

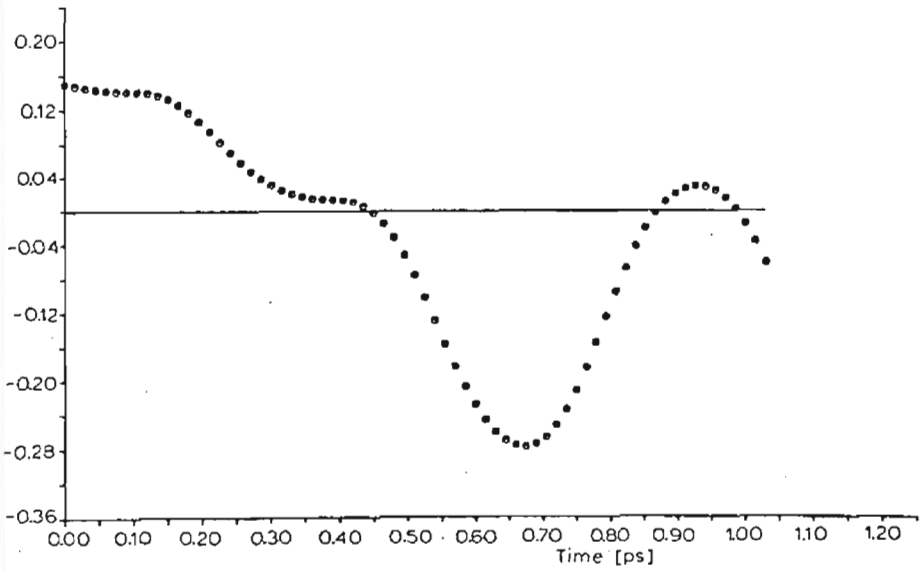

Figure (26)

Tetra algorithm, as for Fig. (14) - Cross correlation

$\langle \underline{V}(t).J(o)\rangle / (\langle V^2(o)\rangle \langle J^2(o)\rangle)^{\frac{1}{2}}$

This correlation does not exist because of symmetry considerations.

The figure shows only the statistical noise.

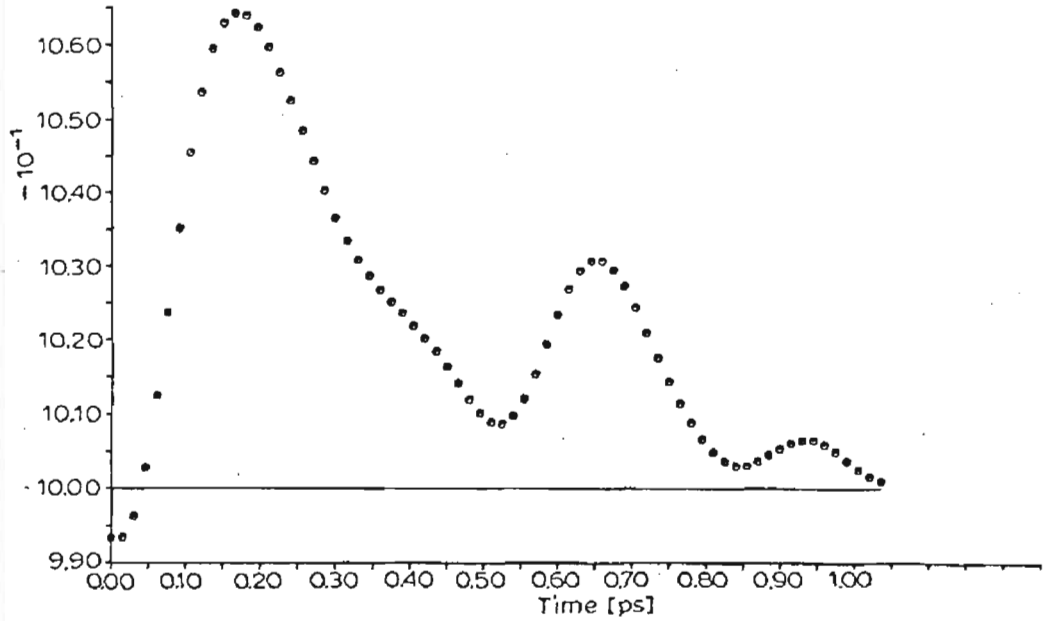

Figure (27)

Tetra algorithm, as for Fig. (14). Cross correlation $\langle V^2(o)\ J^2(t)\rangle / \langle V^2(o)\rangle \langle J^2(o)\rangle$. Apart from noise in the tail it is equal to the c.c.f. $\langle V^2(t)\ J^2(o)\rangle / \langle V^2(o)\rangle \langle J^2(o)\rangle$ as it must be by symmetry considerations.

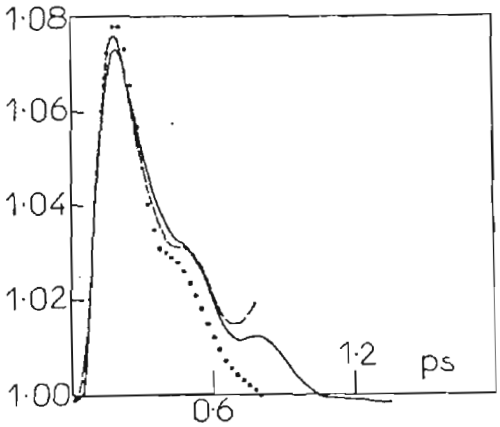

Figure (28)

As for fig. (27): 5 x 5 algorithm, no charges, 12.5 ps running time-span.

—— 3 x 3, no charges, 12.5 ps span.

- - - 3 x 3, no charges, 9 ps span.

Illustrates the small t = o deviation and stable first peak.

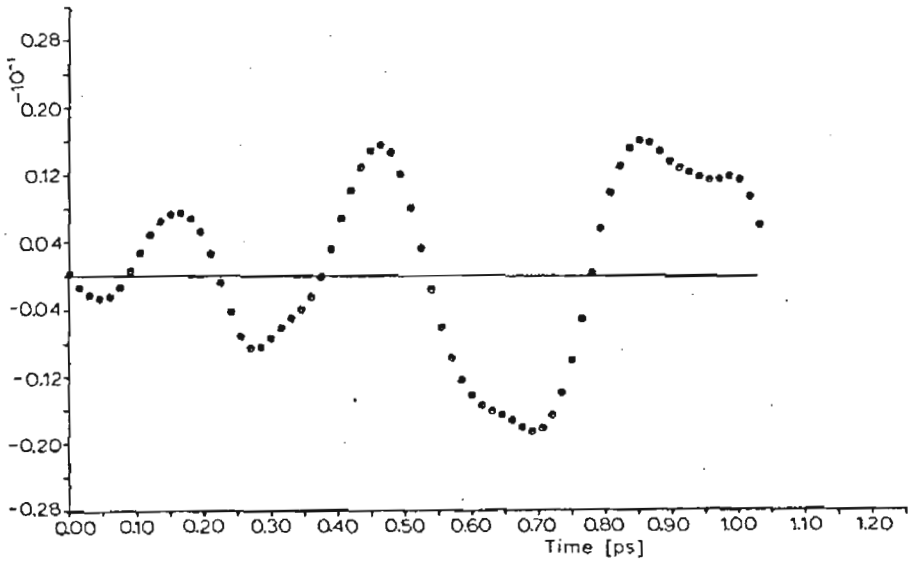

Figure (29)

Tetra algorithm, as for Fig. (14). C.C.F. $\frac{\langle \underline{N}(o).\underline{F}(t)\rangle}{(\langle N^2(o)\rangle\langle F^2(o)\rangle)^{\frac{1}{2}}}$ - c.f. Fig. (26).

TR12 with Charges

Charges were incorporated at atom sites as described earlier. The effect on the equilibrium time correlation functions is not pronounced but is nevertheless significant. This indicates that the dynamics of the liquid are approximately describable in terms of Lennard-Jones parameters but the electrodynamics are nevertheless important for a complete analysis. The inclusion of charge-

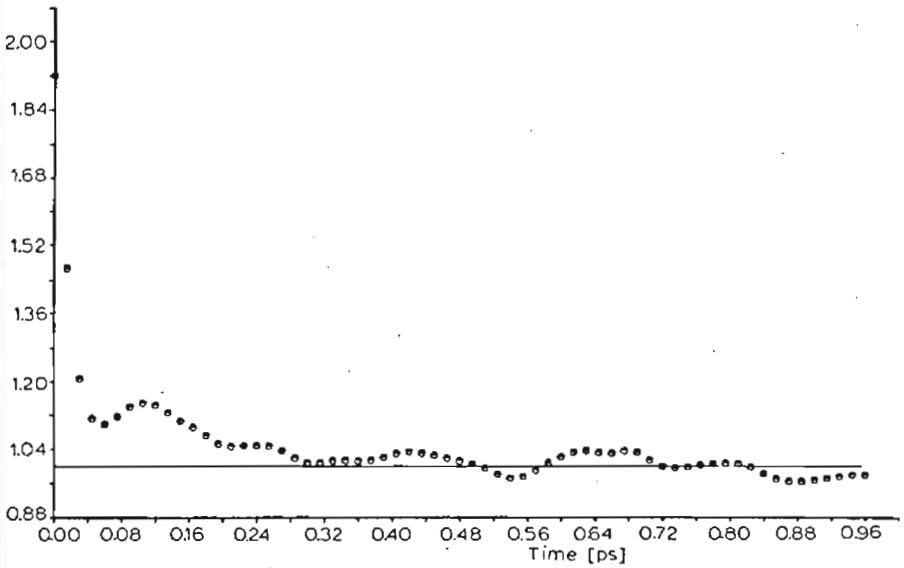

Figure (30)

Tetra algorithm, as for Fig. (14). C.C.F.

$\langle N^2(o)\ F^2(t)\rangle / \langle N^2(o)\rangle\langle F^2(o)\rangle$. c.f. Fig. 27.

Note that at t = o $N^2(o)$ and $F^2(o)$ are correlated.

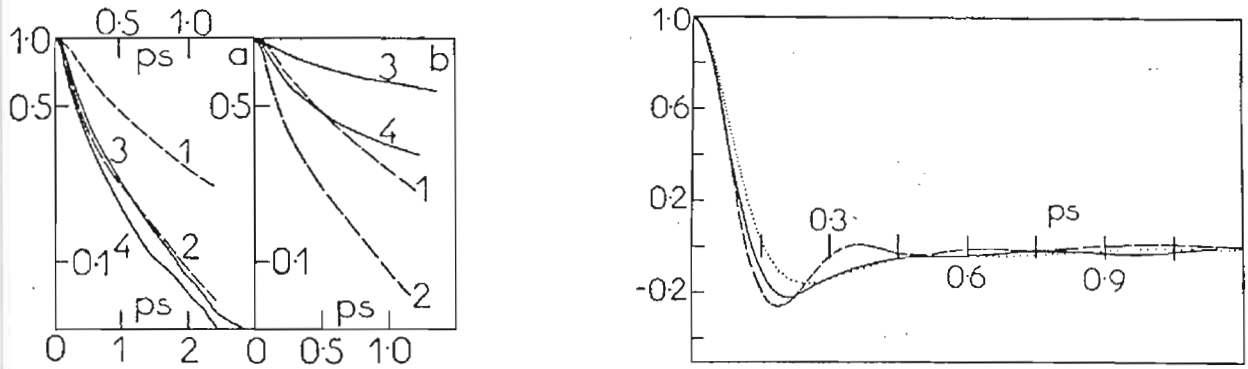

Figure (31)

(a) (1) and (2) P_1 and P_2 a.c.f.'s of $\underline{e}_A$, 3 x 3 potential + charges. (upper abscissa).

(3) and (4) P_1 and P_2 a.c.f.'s of $\underline{e}_A$, 3 x 3 potential no charges (lower abscissa).

Both at 293K, 1 bar.

(b) (1) and (2) as for (a). (3) and (4): 3 x 3 + charges potential at 177K, 1bar.

Figure (32)

Rotational velocity a.c.f.'s of $\dot{\underline{e}}_A(t)$

——— 3 x 3 + charges at 293K, 1bar

- - - 3 x 3 + charges "177K, 1bar.

..... 3 x 3 no charges, at 293K, 1bar.

charge interaction shifts the peak of the far infra-red absorption to higher frequencies and correspondingly increases the P_1 to P_4 correlation times. This is a clear indication that the microwave and N.M.R. relaxation times are increased by long ranged terms of this nature, sometimes to a significant degree. Figs. (31) to (33) are a measure of the effect on some autocorrelation functions of CH_2Cl_2 simulated by the 3 x 3 algorithm. It is interesting to note in Fig. (34) that the multiparticle (microscopic) correlation function:

$$\frac{\langle \dot{\underline{e}}_{Ai}(o) . \sum_{i \neq j} \dot{\underline{e}}_{Aj}(t) \rangle}{\langle \dot{\underline{e}}_{Ai}(o) . \sum_{i \neq j} \dot{\underline{e}}_{Aj}(o) \rangle}$$

decays very similarly to the single particle equivalent at 293K. The auto and 'microscopic' correlation functions do not differ significantly in structure even in the presence of electrodynamic interactions. This is a good indication that single particle theories of the liquid phase can be used to describe multi-particle spectra such as those in far infra-red via a macro correlation theorem.

We remark that with or without charges the TR12 algorithm is not capable of reproducing the observed spectrum. This is not due apparently to our use of a single particle (auto) correlation function based theory as Fig. (34) apparently

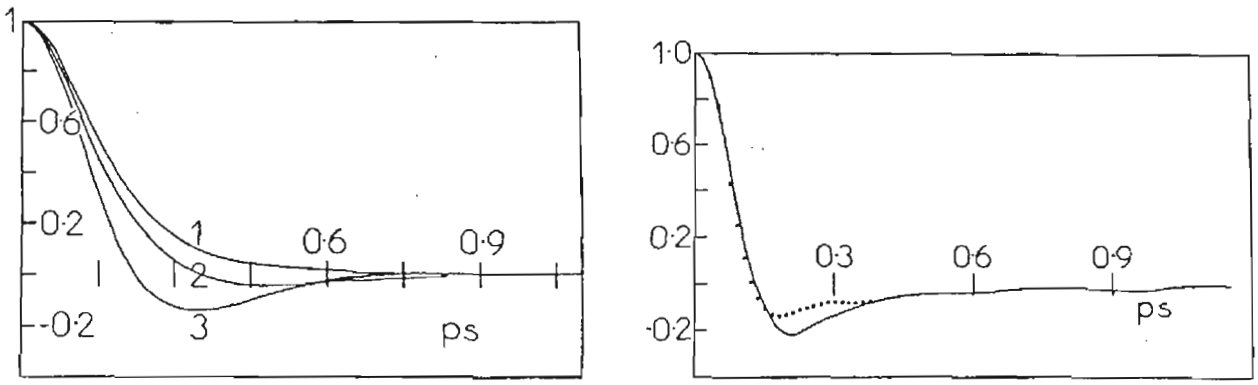

Figure (33)

Comparison of angular momentum a.c.f.'s, lab. frame.

(1) 3 x 3, no charges, 293K, 1bar.

(2) 3 x 3, with charges, 293K, 1bar;

(3) 3 x 3, with charges, 177K, 1bar.

Figure (34)

—— A.c.f. of $\dot{\underline{e}}_A(t)$, 3 x 3 + charges, 293K, 1bar.

• $\langle \dot{\underline{e}}_{Ai}(o) . \Sigma \dot{\underline{e}}_{Aj}(t) \rangle / \langle \dot{\underline{e}}_{Ai}(o) . \Sigma \dot{\underline{e}}_{Aj}(o) \rangle$ computed using a spherical sub-sample containing two or three molecules.

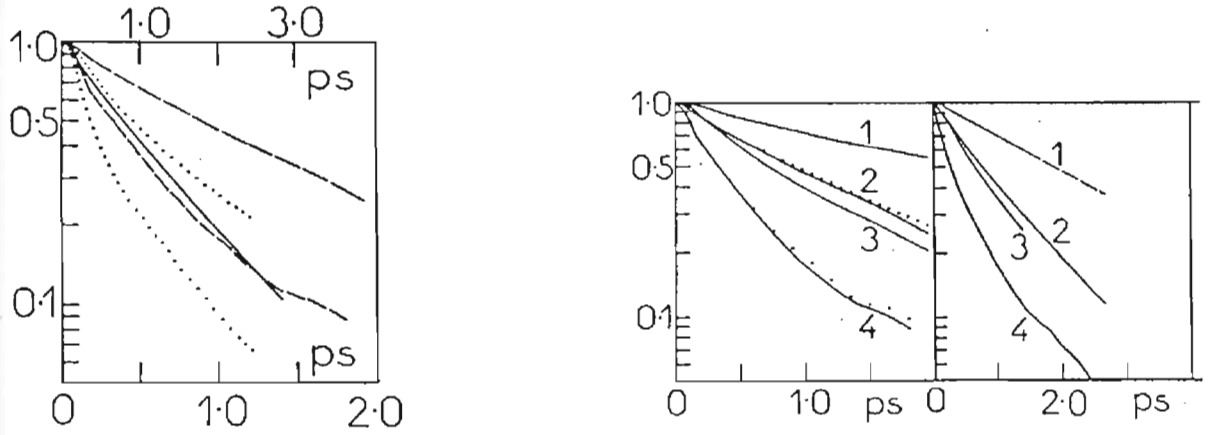

Figure (35)

—— (upper abscissa) P_1 a.c.f. of $\underline{e}_A$, 5 x 5 no charges, 293K, 1bar.

- - - P_1 and P_2 a.c.f.'s of $\underline{e}_A$, 5 x 5 plus charges, 293K, 1bar (lower absicissa).

..... P_1 and P_2 a.c.f.'s of $\underline{e}_A$, 3 x 3 plus charges, 293K, 1bar (lower abscissa).

Figure (36a)

Anisotropy of rotational diffusion: 5 x 5 potential + charges, 293K, 1bar:

(1) P_1 a.c.f. of $\underline{e}_B$; (2) P_1 a.c.f. of $\underline{e}_A$ and , of $\underline{e}_C$;

(3) P_2 a.c.f. of $\underline{e}_B$; (2) P_2 a.c.f. of $\underline{e}_B$ and, • , of e_C.

Figure 36b)

As for Fig. (36a), 5 x 5, no charges. Note P_1 and P_2 of $\underline{e}_C$ are not shown, being very similar to P_1 and P_2 of $\underline{e}_A$.

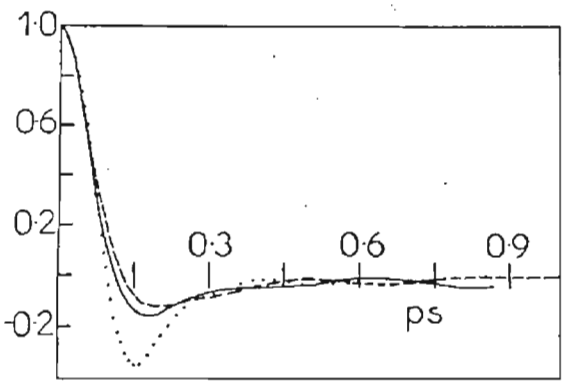

Figure (37)

Rotational velocity a.c.f.'s (of $\underline{e}_A(t)$)

- - - 5 x 5, no charges, 293K, 1bar.

—— 5 x 5, with charges, 293K, 1bar.

..... Computed from far infra-red data on pure liquid CH_2Cl_2.

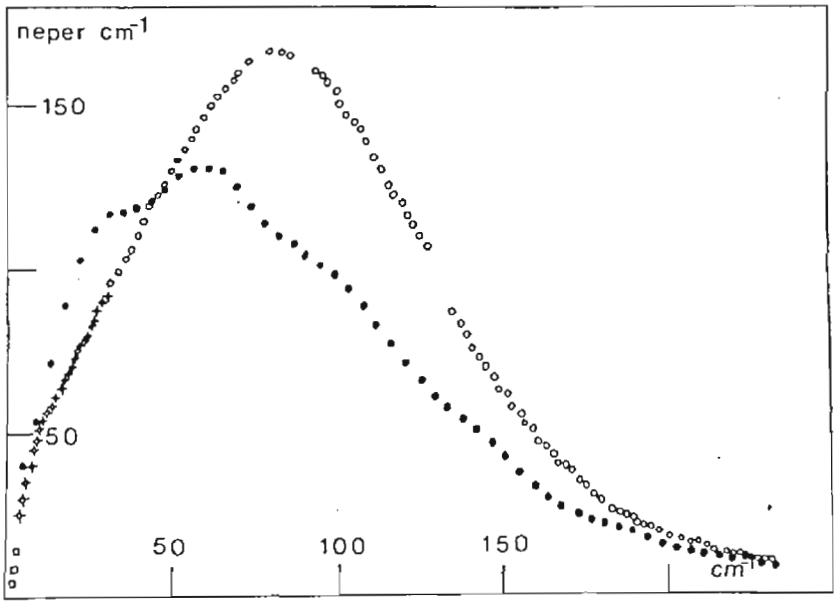

Figure (38)

As for Fig. (7) except that ● denote volues obtained by Fourier transformation of the rotational velocity a.c.f. (of $\underline{\dot{e}}_A(t)$). The F.t. is noisy due to artifacts introduced by the long tail of the a.c.f.

indicates. Improvements are therefore needed in the structure of the pair-potential and particularly in the method used to account for long-ranged forces. As a first step we may attempt to account for the shape of the molecule in more detail by using partial charges in the 5 x 5 atom-atom potential TETRA.

The effect of adding charges on the orientational a.c.f.'s is illustrated in Figs. (35) to (37). The power absorption coefficient $\alpha(\bar{\nu})$ is shifted to higher frequencies as illustrated in Fig. (38), but it is still below the observed peak at 80 cm^{-1}.

SECTION 3

Discussion and Suggestions for Further Work.

In this paper we have described how it is now possible to use the technique of molecular dynamics simulation to transform intermolecular potential parameters such as σ and ϵ/k directly into a wide variety of theoretical correlation functions, and by Fourier transform into spectra of the liquid state. As computer power and accessibility increases this will become routine. It is therefore apparent that a multi-technique approach to liquid state spectroscopy must also become routine to deal with the catholicity of the new hypotheses embodied in computer simulation.

The liquid should be investigated at a given state point from as many different viewpoints as possible and these state points should cover the complete range from triple point to critical point using pressure as well as temperature and viscosity as a variable.

The whole range of spectra and simulated spectra should be used with one major purpose in mind. That is to improve our analytical understanding of the way in which molecules interact in the liquid state of matter. In this respect it is particularly important to structure the molecular dynamics algorithms in such a way that the results (whenever available) of ab initio calculations can be used in the forces loops. The model potentials should be tried out on useful thermodynamic data such as the second dielectric virial coefficient B_ε and <u>third</u> pressure virial C_p. It is often the case that model potentials which seem to work well produce the <u>wrong sign</u> for B_ε but on the other hand atom-atom + charges models seem to work well compared with ab initio calculations as pointed out recently by van der Avoird et al [10].

In this paper we have made a limited foray into the dynamic properties of liquid CH_2Cl_2 with two different atom-atom potentials which can be improved significantly if the necessary B_ε data were to become available over a wide temperature range. The zero-THz range of frequencies is also a sensitive test of the way that molecules interact and it is known that the spectrum of CH_2Cl_2 changes dramatically in dilute, supercooled decalin solution to cover an enormous range of frequency of over a dozen decades (the α, β and γ processes of Reid and Evans). We have investigated the effect of adding charges to the core 5 x 5 (and 3 x 3) atom-atom potentials. Their role is significant, and using centre-of-mass to centre of mass cut-off it seems that the periodic boundary conditions are not problematical even using as few as 108 molecules. For a proper calculation of many body correlation functions we would require ideally an order of magnitude more molecules. Our calculations on cross correlation functions are restricted at present to within a microscopic sphere of about 8 Å radius, containing only about twenty molecules.

ACKNOWLEDGEMENTS

It is a pleasure to acknowledge the advice and help of Professor K. Singer and the SRC CCP5 group with the algorithms TR12 and TETRA. SRC is also thanked for financial support to MWE and the Italian CNR for support to MF in the context of the EMLG pilot project.

REFERENCES

1.P.N. Brier and A. Perry, Adv.Mol.Rel.Int.Proc., 13, 1978,46.

2.M.W. Evans, G.J. Evans, W.T. Coffey and P. Grigolini, "Molecular Dynamics", Wiley/Interscience, N.Y., to be published, Chapters 6 and 12, covering the EMLG Pilot Project.

3.M.W. Evans and J. Yarwood, Adv.Mol.Rel.Int.Proc., in press, "Proposals for a Collaborative Project on Molecular Dynamics".

4.I.R. McDonald, communication.

5.For energy of vapourization see "Selected Values of Chemical Thermodynamic Properties", 1961, p.588. At 760mn Hg, 313K ΔH = 6.69 kcal $mole^{-1}$; ΔS = 21.4 cal $(mole\ K)^{-1}$.

6.K. Singer, J.V.L. Singer and A.J. Taylor, Mol. Phys., 37, 1979,1239.

7.R. Del Re, J.Chem.Soc., 36, 1958,101.

8.P.S.Y. Cheung, Mol.Phys., 3, 1977, 519.

9.C. Brot, "Dielectric and Related Molecular Processes", Vol.2, 1975, p.1. Chem. Soc. Specialist periodical report, senior reporter: M. Davies.

10.A. van der Avoird, P.E.S. Wormer, F. Mulder and R.M. Berns, "Ab Initio Studies of the Interactions in van der Waals Molecules", in Topics in Current Chemistry, 93", ed. Dewar et al, Springer Verlag, Berlin, 1980.